Indian Journal of Chemistry
Vol. 56A, December 2017, pp. 1285-1292

Rapid synthesis of Tb^{3+}-doped gadolinium oxyhydroxide and oxide green phosphors and their biological behaviour

Saima Wani[a], Shafquat Majeed[b,c] & S A Shivashankar[b,d,*]

[a]Department of Biochemistry, Indian Institute of Science, Bangalore 560 012, India
[b]Materials Research Centre, Indian Institute of Science, Bangalore 560 012, India
[c]Department of Nanotechnology, University of Kashmir, Hazratbal, Srinagar 190 006
[d]Centre for Nano Science and Engineering, Indian Institute of Science, Bangalore 560 012, India

Email: shivu@cense.iisc.ernet.in

Received 13 August 2017; revised and accepted 17 November 2017

Green phosphors based on terbium doped GdOOH and Gd_2O_3 powders are prepared through a rapid microwave-assisted solution based method using ethanol as a solvent and without using any surfactants. The as-prepared Tb^{3+}:GdOOH powders are crystalline and show a flower-like morphology comprising many two-dimensional flake-like structures. The as-prepared powders show good luminescence properties under UV excitation and their conversion to Tb^{3+}:Gd_2O_3 by annealing takes place at modest temperatures. A considerable increase in luminescence intensity is observed for the annealed powders, which is ascribed to phase change from oxyhydroxide to oxide as well as an increase in crystallinity as a result of annealing. Cytotoxicity studies reveal that the as-prepared powders show considerable toxicity towards the cells, whereas the annealed powders do not hamper the cell growth.

Keywords: Rare earths, Self-assembly, Nanomaterials, Optical materials, Photoluminescence, Phosphors, Green phosphors, Terbium doping, Gadolinium, Oxyhydroxides, Oxides

Luminescent solid materials that can absorb and convert certain types of energy into light are called phosphors.[1] Rare earth compounds, among all kinds of phosphors, show excellent optical properties due to the presence of *f*-orbital electrons and represent an important and attractive class of materials for phosphor applications. With a number of *f*-orbital configurations available, lanthanide (Ln) ions can exhibit sharp fluorescent emissions via intra-configurational *f*-*f* or 4*f*-5*d* transitions and thus are widely used as emitting species or centres in many phosphors. Since the 4*f* shell of trivalent lanthanide ions is well shielded by the filled 5*s* and 5*p* orbitals, the energy levels of the 4*f* electrons are not influenced much by the surrounding environment of the lanthanide ion. Thus, the lanthanide ion behaves to a large extent as a free ion and the crystal field effect is only a weak perturbation. This leads to sharp lines (similar to atomic spectra) observed in the electronic spectra of lanthanides[2]. This weak perturbation is also responsible for the fine structure observed in lanthanide spectra.

However, the intensity of these 4*f*-4*f* transitions is weak since these transitions are not allowed by Laporte selection rule (in a molecule with a centre of symmetry, transitions within a given set of *p*, *d* or *f* orbitals, i.e., those which only involve a redistribution of electrons within a given subshell are forbidden). Further, because of the weak crystal field interaction of these deep lying *f*-electronic levels, the relaxation of this selection rule is less effective for lanthanide ions than for transition metal ions. To overcome this limitation, rare earth ions are doped in low concentrations into a suitable host lattice to yield highly luminescent materials. In Ln^{3+}-doped inorganic materials, the rigid host lattice provides a steady microenvironment for Ln^{3+} activator ion. Some host materials or other co-doping ions even possess a higher absorption coefficient than Ln^{3+} emitter, which leads to an efficient energy transfer to the activator Ln^{3+} ions, leading to higher quantum yields. In addition, by changing the doped Ln^{3+} activator ion in a host lattice, the emission colour can be easily tuned, e.g., doping of Eu^{3+} ions in Gd_2O_3 gives a red emission whereas a green emission is observed when Tb^{3+} or Dy^{3+} ions are doped in the Gd_2O_3 host lattice.[3–5] Doping also has an added advantage of reducing the concentration quenching, wherein the emission centres, if close to each other, interact by non-radiative cross relaxation processes, leading to a

lower quantum yield.[6] Moreover, compared with lanthanide chelates, quantum dots (QDs), and organic dye molecules, rare-earth based luminescent materials hold all the advantages of a large Stokes shift, a sharp emission spectrum, a long lifetime, high chemical/photochemical stability, low toxicity, and reduced photobleaching[7,8], which makes them promising phosphor materials for a wealth of applications in the fields of lasers, displays, sensors, solar cells, electroluminescent devices, and biomedical research.[9–13]

Although there are many reports available on the luminescence properties of rare earth ions doped in a Gd_2O_3 host, only a few reports are available on the luminescent properties of rare-earth ions doped in GdOOH host.[3,4,14–16] This is also due to the fact that GdOOH phase is obtained by partial dehydration of $Gd(OH)_3$ phase, which often contains traces of impurities either from oxide or hydroxide phase; there are no reports on its direct synthesis. In this paper, we present a facile, one-step, microwave-assisted method for the synthesis of luminescent Tb^{3+} doped GdOOH microspherical hierarchical structures and their strong luminescent properties. Thermal conversion to Tb^{3+}:Gd_2O_3 phosphors takes place at modest temperatures with improved luminescence properties while retaining the precursor morphology. Recently, considerable interest has been paid to the use of rare-earth based nano-phosphors in biomedical applications such as cell labelling or bioimaging and in MRI contrast imaging.[17–20] In view of this, cytotoxicity studies of the as-prepared and annealed powders were carried out to investigate their potential in these advanced applications.

Materials and Methods

The stoichiometric amounts of $Ln(acac)_3.xH_2O$ (Ln = Gd and Tb) precursors used for preparing various Tb^{3+} doped GdOOH microspheres are shown in Table S1 (Supplementary Data). In a typical experiment, for the synthesis of 1 mol% Tb^{3+} doped GdOOH powder sample, 0.003 g of $Tb(acac)_3.xH_2O$ and 0.297 g of $Gd(acac)_3.xH_2O$ (representing a molar ratio of 1:99 with respect to Tb:Gd respectively), were dissolved in 50 mL ethanol and subjected to microwave irradiation in a single-mode microwave reactor (2.45 GHz, Discover, CEM, USA), equipped with a pressure sensor and an optical fiber temperature sensor. The reaction mixture was heated to 150 °C in 2.1 min (run time) and kept at this temperature for another 5 min (hold time); thus the overall reaction time is 7 min. Microwave power was then switched off and the reaction vessel was allowed to cool naturally to room temperature. The milky white suspension thus obtained was subjected to centrifugation at 6000 rpm to separate the white precipitate from the solution. The precipitate was washed with ethanol several times and dried at 70 °C for 10 h in a hot-air oven for further analysis.

Characterization

X-ray powder diffraction (XRD) was carried out on the powder samples (Cu K_α, λ = 1.5405 Å, PANalytical X'Pert PRO diffractometer, 2θ range from 10° to 70°). Field-emission scanning electron microscopy was used to examine the morphology and microstructure of the samples (FESEM, Carl-Zeiss). SEM samples were prepared by simply dispersing powder samples onto to a carbon film mounted on an aluminium specimen holder. The photoluminescence (PL) spectra of the samples were recorded at room temperature with excitation at 325 nm wavelength (He-Cd laser, Horiba Jobin-Yvon LabRAM HR 100 Raman instrument, CCD detector). Different laser operating powers were used with an acquisition time of 5 s, and the LMU-40x-NUV objective was used for recording the data. There is no direct way of measuring the laser power on the sample surface in our instrumental setup, and hence since there is a very small distance between the sample and the measurement lens, it was assumed that all of the power the laser supplied (mentioned), was incident on the sample surface.

Cell viability assay

The 3-(4,5-dimethylthiazol-2-yl)-2,5-diphenyltetrazolium bromide (MTT) assay was carried out to assay the effect of the Tb^{3+}:GdOOH and Tb^{3+}:Gd_2O_3 powders on cell viability. HCT116, a colorectal cell line, was plated at 3.0×10^3 cells/well in a 96-well plate format. After 24 h of plating, the cells were treated with the indicated concentrations of the as-prepared Tb^{3+}:GdOOH powders and Tb^{3+}:Gd_2O_3 (annealed). MTT (20 µL of 5 mg/mL in PBS) was added 48 h after rare-earth powders delivery. MTT is a tetrazolium salt that is reduced by the metabolically active cells, partially by the action of the dehydrogenase enzymes, to liberate reducing equivalents like NADH and NADPH. As a by-product of the reaction, purple coloured formazan crystals were formed by the metabolically active cells which were solubilized and quantified by spectrophotometric means. After 3 h of MTT addition, the media was removed completely from the wells and 200 µL of dimethyl sulfoxide was added to dissolve the formazan crystals.

The absorbance was measured at a wavelength of 570 nm in an enzyme-linked immunosorbent assay reader. The viability of control untreated cells was considered as 100%. Significance was calculated by ANOVA and the p-values are indicated ("ns" = not significant, "*" p <0.05, "**" p <0.01, "***"p <0.001).

Results and Discussion

XRD characterization

The XRD patterns of GdOOH and the as-prepared Tb^{3+} doped GdOOH powders are shown in Fig. 1(a) and the XRD patterns of the annealed products at 600 ºC at 2 h, i.e., Gd_2O_3 and Tb^{3+} doped Gd_2O_3 powders are shown in Fig. 1(b). In the case of the as-prepared product, all the peaks could be indexed to monoclinic "intermediate phase" of GdOOH based on published reports[3,4,21] and all the peaks of annealed Tb^{3+}:Gd_2O_3 powder could be indexed readily to the cubic phase of Gd_2O_3 (JCPDS 12–0797). The small ionic size difference between Tb^{3+} and Gd^{3+} ions does not cause any appreciable change in size of the unit cell and hence is not reflected in the XRD pattern (no shifting of peaks). This is also the reason why these rare-earth dopant ions can easily substitute rare-earth ions of the host ions. The detailed account of the position of these dopants in monoclinic and cubic systems is given in our earlier work.[3]

Morphology and microstructure

The morphology of the as-prepared Tb^{3+} doped GdOOH powder samples is shown in Fig. 2(a) and 2(b) respectively. As can be seen from the figure, the as-prepared sample consists of 3D-spheres having dimensions in the micrometre range and shows a flower-like morphology. A close examination of these flower-like spheres in Fig. 2 (b) shows that each one consists of a large number of 2D-flakes assembled together to form these spheres and each flake (inset in Fig. 2(b)), in turn, consists of a large number of nanoparticles assembled together, thus, presenting a three degree hierarchy in its structure. While the reason for the formation of such morphology is not clear, it is surmised that it is the kinetics of the reaction system that leads to the formation of these unusual structures, since the entire reaction/structure formation completes in only seven minutes. On the other hand, from the thermodynamic

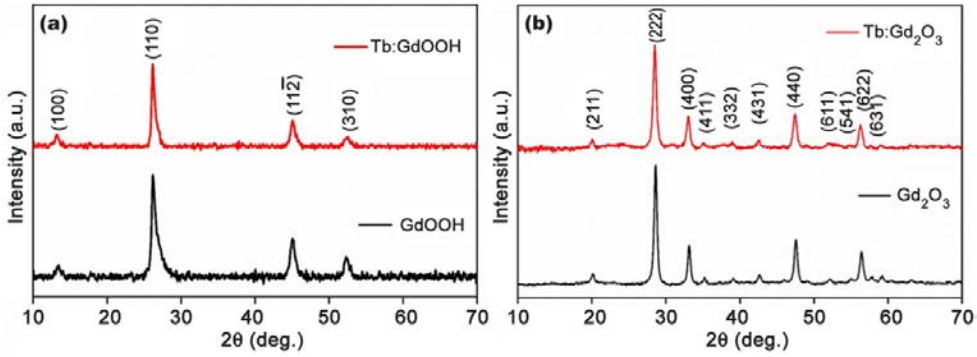

Fig. 1 — (a) Powder XRD patterns of as-prepared Tb^{3+}-doped GdOOH and annealed Tb^{3+}-doped Gd_2O_3 product. (b) XRD patterns indexed to GdOOH and Gd_2O_3 phases, respectively.

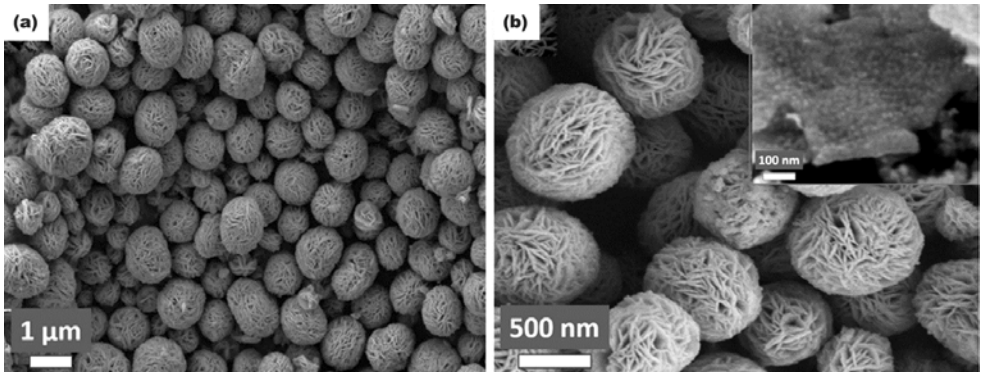

Fig. 2 — (a) Morphology of the as-prepared Tb^{3+}-doped GdOOH powders showing the presence of 3D-spherical structures of micrometre dimensions. (b) A high magnification image of these structures. [Inset in (b) shows a single nanoflake, of which these spherical structures are made up of.]

view point, it may be inferred that the morphology arises from some sort of layer-by-layer assembly (energy minimization). However, as it occurs very fast, it appears that there is not enough relaxation time for a "proper" arrangement. Nevertheless, the flakes assemble together to form the globular structures. The driving force for the formation of spherical assemblies seems to be the minimization of energy. The morphology of the oxide phase does not change and is similar to that of the parent GdOOH phase. It must be noted that the morphology of the annealed product, i.e., Tb^{3+}:Gd_2O_3 does not change after the annealing process and it resembles the same spherical morphology of as-prepared Tb^{3+}:GdOOH spheres. (Supplementary Data, Fig. S1)

Photoluminescence properties

The room temperature photoluminescence emission spectrum of 5 mol% Tb^{3+} doped GdOOH powders under an excitation wavelength of 325 nm is shown in Fig. 3(a). The inset of Fig. 3(a) shows the intense green colour of the powder under UV excitation. The emission spectrum displays four emission peaks between 450 and 650 nm, which are assigned to the intra-configurational *f-f* transitions within Tb^{3+} ions.[22,23] The origin of various emission lines is shown in the corresponding energy level diagrams of the Tb^{3+} (Fig. 3(b)). The emission lines correspond to $^5D_4 \rightarrow {}^7F_6$ (489 nm), $^5D_4 \rightarrow {}^7F_5$ (543 nm), $^5D_4 \rightarrow {}^7F_4$ (584 nm) and $^5D_4 \rightarrow {}^7F_3$ (621 nm), respectively. The emission peak at 489 nm ($^5D_4 \rightarrow {}^7F_6$) is an allowed electric dipole transition ($\Delta J = 2$), while the 543 nm ($^5D_4 \rightarrow {}^7F_5$) emission line, which is more intense than other transitions, corresponds to the allowed magnetic-dipole transition ($\Delta J = 1$), and is responsible for the green colour of the powder under UV excitation.[23-24]

The PL emission spectra of the Tb^{3+}:GdOOH powder samples with different Tb^{3+} doping concentrations are shown in Fig. 4(a). Figure 4(b) represents the variation

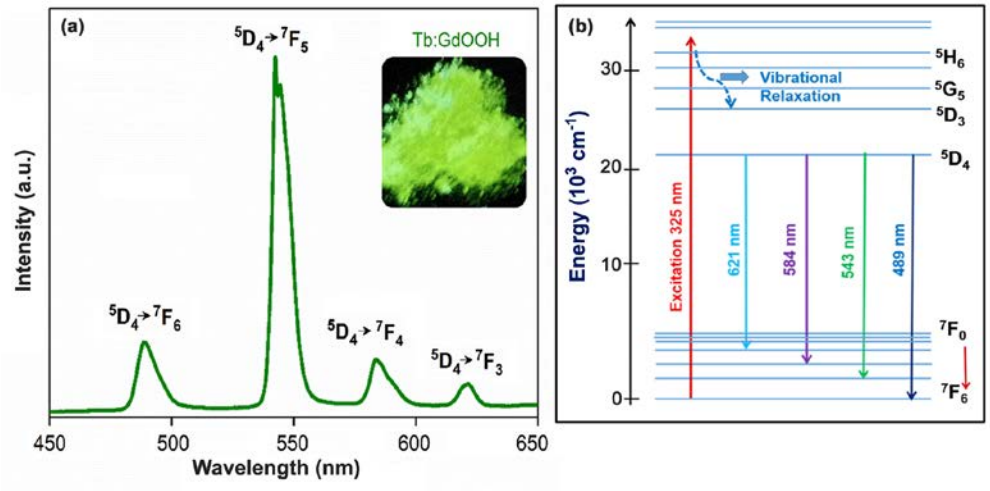

Fig. 3 — (a) PL emission spectrum of the Tb^{3+}:GdOOH powder (5 mol% Tb^{3+}) showing a strong green emission under an excitation wavelength of 325 nm. [Inset shows the strong green luminescent glow of the powder sample under UV excitation]. (b) Energy level diagram for Tb^{3+} ion showing the origin of various emission lines.

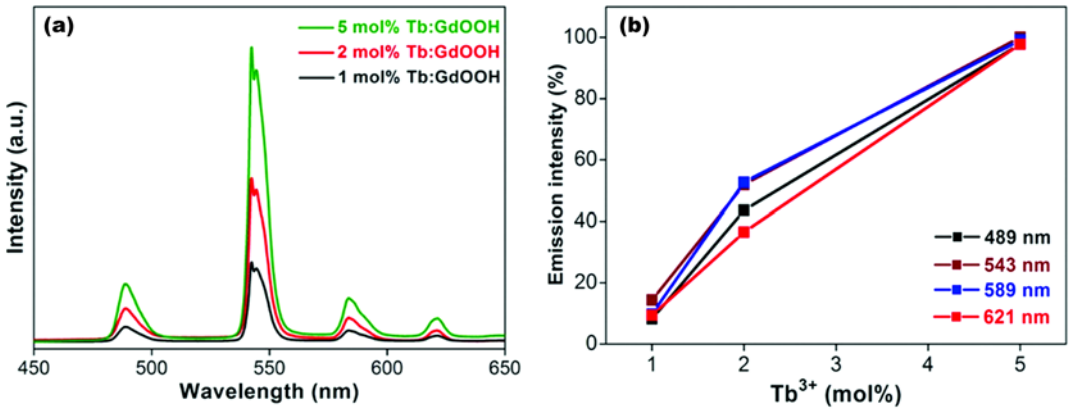

Fig. 4 — (a) Variation of PL emission intensity with Tb^{3+} doping concentration. (b) Variation in emission intensity of 489, 543, 584 and 621 nm peaks with increasing Tb^{3+} concentration. [The maximum intensity is assumed to be 100% for 5 mol% Tb^{3+}-doped GdOOH samples].

in the PL intensity of individual peaks at 489, 543, 584 and 621 nm (Tb^{3+}:GdOOH) with increasing dopant concentration. It can be seen that, in the case of Tb^{3+} doped GdOOH powders, the PL emission intensity increases almost linearly with an increase in Tb^{3+} doping concentration (1%, 2%, 5%), which is due to the increase in the number of active emission centres as the doping concentration is increased.

To study the distribution of Tb^{3+} dopants within GdOOH host, element mapping was carried out by SEM energy-dispersive X-ray spectrometry (SEM/EDS) (Fig. 5), which shows that Tb^{3+} ions are distributed uniformly in GdOOH host lattice; this reduces the concentration quenching, thereby increasing the PL emission intensity.

The PL emission spectra of Tb^{3+}:GdOOH (1 mol%) powder samples at different laser pump powers were recorded to investigate its stability (Fig. 6(a)). The variation in the emission intensity of the Tb^{3+} peaks at 489, 543, 589 and 621 nm (Tb^{3+}:GdOOH) with laser power is shown in Fig. 6(b). It is clear from the Fig. 6(b) that, in the case of Tb^{3+}-doped GdOOH powders, the emission intensity increases almost linearly up to a laser power value of 3.5 mW, whereas the intensity drops at higher values of laser power indicating that it is not stable at higher laser power. This reduction in emission intensity at higher power values can be attributed to local heating caused by the laser beam, including phase change from crystalline GdOOH to amorphous Gd_2O_3, since crystalline phase of Tb^{3+}:Gd_2O_3 is formed at higher temperatures (≈ 600 ºC in the present case), and, such temperatures cannot be attained by laser heating. The PL emission spectrum of the powder samples annealed at 600 ºC (5 mol% Tb^{3+}:Gd_2O_3) is shown in Fig. 6(c), which also includes the PL emission spectrum of the corresponding as-prepared Tb^{3+}:GdOOH as reference. As expected, the emission intensity of the annealed powders is much higher, and the peaks are less broad and show a fine structure. This observed change in intensity is due to change in phase from monoclinic (as-prepared Tb^{3+}:GdOOH) to cubic (annealed Tb^{3+}:Gd_2O_3); it is well known that emission of rare-earth dopants in cubic phase is much higher than in the monoclinic phase.[3] The absence of any organic capping agents (which are known to be efficient quenching agents), and increase in crystallinity after annealing (which leads to fewer defects, thus preventing relaxation through non-radiative processes) are the other factors that increase the PL emission in annealed samples. Further, the emission peaks of the annealed samples have a fine structure due to the influence of surrounding small crystal field on the *f*-orbital energy levels, which causes their splitting. This effect is more enhanced in the case of the annealed samples because the Tb^{3+} dopants are in proper lattice sites, whereas, in the case of as-prepared powders these dopants are in a more or less disordered matrix.

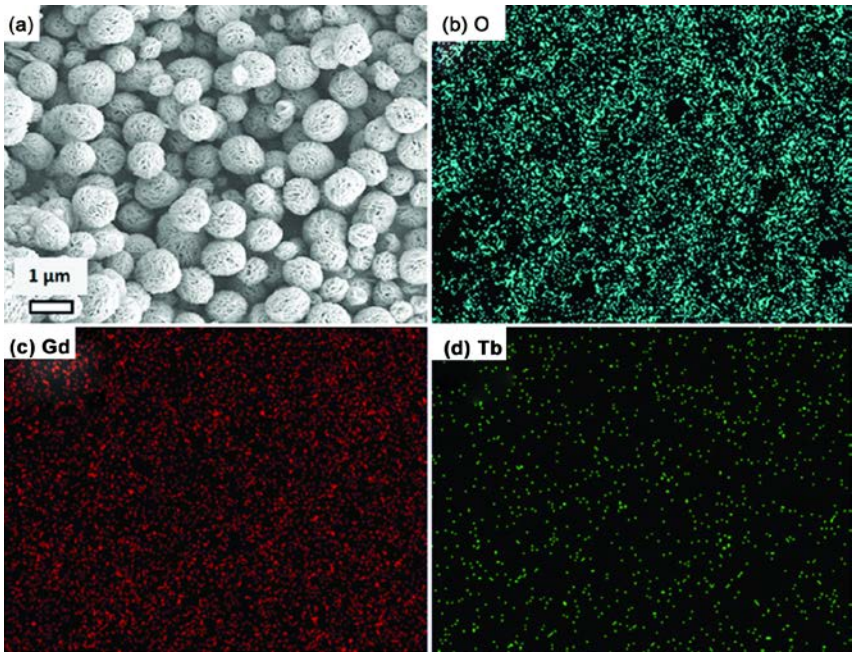

Fig. 5 — (a) SEM image of Tb^{3+}:GdOOH powder, and (b-d) the corresponding SEM-EDS elemental maps for O K_α, Gd L_α and Tb L_α showing a uniform distribution of Tb^{3+} dopant ions in the GdOOH host lattice. [5 mol% Tb^{3+}-doped GdOOH sample was used for obtaining the elemental maps].

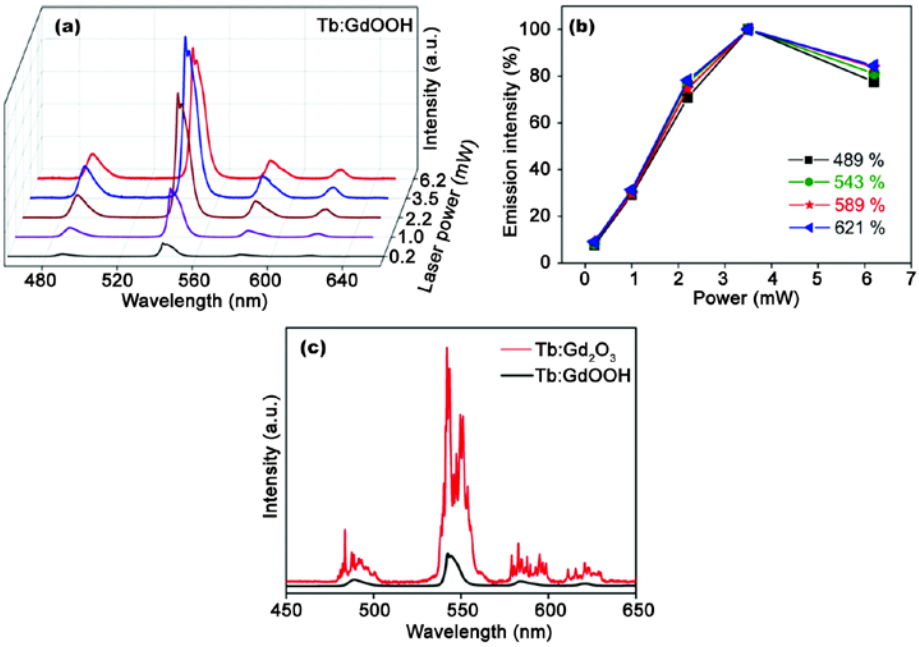

Fig. 6—(a) PL spectra of 1 mol% Tb^{3+}:GdOOH powder samples at different laser pump powers. (b) Variation of individual peak intensities at 489, 543, 589 and 621 nm for Tb^{3+}:GdOOH with increasing laser power. [The maximum intensity of Tb^{3+} peaks at 489, 543, 589 and 621 nm is assumed to be 100% at 3.5 mW]. (c) PL emission spectra of as-prepared 5 mol% doped Tb^{3+}:GdOOH sample and after annealing in air at 600 °C. [All measurements were made with excitation at 325 nm].

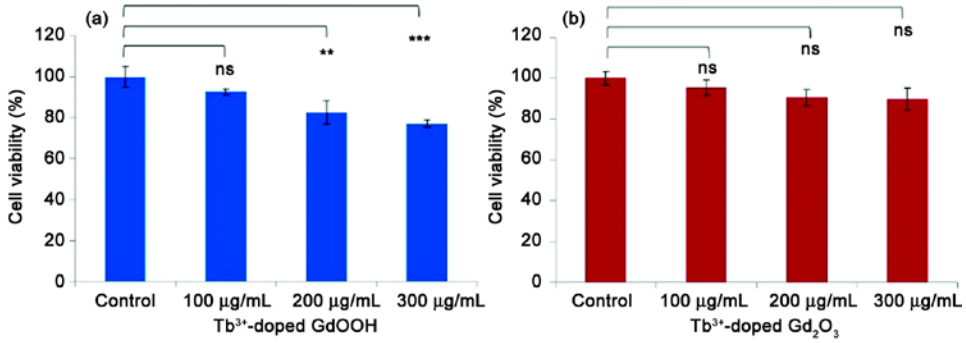

Fig. 7—(a) Cell viability upon treatment with different concentrations of Tb^{3+}-doped GdOOH powders. [There is a subtle reduction in cell viability for higher concentrations used, e.g., 200 and 300 µg/mL]. (b) Cell viability upon treatment with different concentrations of Tb^{3+}-doped Gd_2O_3 powders. [There is no change in cell viability in the range of 100 µg/mL to 300 µg/mL. Significance was calculated by ANOVA].

This is due to fast reaction kinetics of the synthesis process (coupled with a low synthesis temperature of 150 °C). As a consequence, the crystallite size is small in as-prepared powders, making the fraction of Tb^{3+} ions on the surface quite significant. This also leads to local distortions or crystal imperfections, which can cause peak broadening as observed in as-prepared powders.

Toxicity studies

Recently, much attention has been devoted to rare-earth based/doped nanomaterials for their biomedical use, such as in fluorescent cell labelling, PET, MRI imaging, etc. The use of Gd-based rare-earth nanomaterials as positive contrast agents in MRI imaging is gaining momentum since a nanoparticle carries a greater payload of Gd^{3+} ions than a bulky Gd-chelate complex that is commonly used to increase contrast in MRI images.[24] However, to realize these potential applications, cellular response of these materials is very important and must be evaluated to verify that these materials are non-toxic and biologically compatible. With that in mind, we investigated the effect of as-prepared Tb^{3+}:GdOOH and annealed Tb^{3+}:Gd_2O_3 powders on the viability of HCT116, a colorectal cell line.

The viability of cells after 48 h, when treated with different concentrations of as-prepared and annealed powders, is shown in Fig. 7. There is appreciable

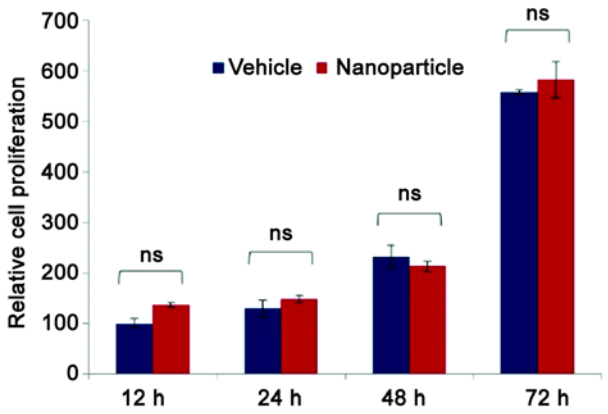

Fig. 8—Cell viability upon treatment with the highest concentration of annealed Tb^{3+}:Gd_2O_3 powders over a course of time as indicated. [There is no change in cell viability between control and Tb^{3+}:Gd_2O_3 powders. Significance was calculated by ANOVA].

reduction in cell viability for cells treated with Tb^{3+}:GdOOH, whereas cell growth remains unaffected after the cells are treated with Tb^{3+}:Gd_2O_3 powders. The reason for this behaviour can be the presence of capping agents in as-prepared samples, whereas annealed samples are pristine as shown by the IR analysis (Supplementary Data, Fig. S2). However, for the annealed sample, cytotoxicity studies with respect to the duration of exposure to cells are also important, since a material can show toxicity over a period of time.

It is clear from Fig. 8 that no long-term cytotoxicity effects were observed even after 3 days, during which HCT116 cells were treated with the highest tested concentration (300 μg/mL herein) of annealed Tb^{3+}:Gd_2O_3 powders. The reason for the low toxicity of annealed powders beside their pristine nature is due to their high crystallinity, that holds the constituent ions (Gd^{3+} and Tb^{3+} in the present case) firmly in place in a crystalline nanoparticle, and, this in turn minimizes their leakage preventing any cytotoxic response. This further substantiates that rare-earth based probes in their pristine form have no long term toxicity towards cells and may find use in biomedical applications.

Conclusions

Spherical hierarchical structures of Tb^{3+}:GdOOH were prepared by a rapid solution-based, microwave-assisted route, without using any surfactants. These spherical structures are nearly monodisperse and display a typical hierarchy in structure. Tb^{3+}-doped GdOOH powder samples display good, bright green photoluminescence and green being one of the primary colours, this material may prove useful for the fabrication of white light LEDs. Tb^{3+}:GdOOH can be converted to the corresponding oxide structure at modest temperatures with the spherical morphology intact, but with enhanced emission characteristics, making them promising phosphor material with prospects in a variety of applications. Cytotoxicity studies reveal that the as-prepared powder samples show appreciable toxicity towards cell growth, whereas both concentration and time dependent studies of the annealed powders show that they are not cytotoxic. If the size of these spheres can be tuned down to 50-100 nm, they may be useful as multimodal agents in bioprobe applications such as bio-labelling and MRI. Further studies towards this shall be taken up in the future.

Supplementary Data

Supplementary data associated with this article is available in the electronic form at http://www.niscair.res.in/jinfo.ijca/IJCA_56A_(12)1285-1292_SupplData.pdf

Acknowledgment

The authors acknowledge gratefully the Centre for Nano Science and Engineering (CeNSE) and the Advanced Facility for Microscopy and Microanalysis (AFMM) of the Indian Institute of Science, Bangalore, India, for supporting analyses by photoluminescence, SEM, and IR. SM thanks the University Grants Commission (UGC), New Delhi, India, for the award of a research fellowship.

References

1 Butler K H, *Fluorescent Lamp Phosphors: Technology and Theory*, (Pennsylvania State University Press, Philadelphia) 1980.
2 Binnemans K & Görller-Walrand C, *Chem Phys Lett*, 235 (1995) 163.
3 Majeed S & Shivashankar S A, *J Mater Chem C*, 2 (2014) 2965.
4 Majeed S & Shivashankar S A, *Mater Lett*, 125 (2014) 136.
5 Petoral R M, So F, Klasson A, Suska A, Fortin M A, Ka P & Engstro M, *J Phys Chem C*, 113 (2009) 6913.
6 Dexter D & Schulman J, *J Chem Phys*, 22 (1954) 1063.
7 Nichkova M, Dosev D, Gee S J, Hammock B D & Kennedy I M, *Anal Chem*, 77 (2005) 6864.
8 Goldys E M, Drozdowicz-Tomsia K, Jinjun S, Dosev D, Kennedy I M, Yatsunenko S & Godlewski M, *J Am Chem Soc*, 128 (2006) 14498.
9 Eliseeva S V & Bünzli J-C G, *Chem Soc Rev*, 39 (2010) 189.
10 Carlos L D, Ferreira R A S, Bermudez V D Z & Ribeiro S J L, *Adv Mater*, 21 (2009) 509.
11 Feldmann C, Jüstel T, Ronda C R & Schmidt P J, *Adv Funct Mater*, 13 (2003) 511.
12 Cheng L, Yang K, Li Y, Chen J, Wang C, Shao M, Lee S-T & Liu Z, *Angew Chem Int Ed Engl*, 50 (2011) 7385.
13 Stouwdam J W & Veggel F C J M Van, *Nano Lett*, 2 (2002) 733.

14 Chang C, Zhang Q & Mao D, *Nanotechnology*, 17 (2006) 1981.
15 Almeida M S de, Santos M A B dos, Gonçalves R de F, Santos M R de C, Marques A P de A, Longo E, La Porta F de A, Pinatti I M, Silva M D P & Godinho M J, *Mat Res*, 19 (2016) 1155.
16 Zhang C, Dai R, Sui Z, Chen Q, Wang Z, Yuan X, Zhang Z & Ding Z, *Chem Phys Lett,* 612 (2014) 138.
17 Majeed S & Shivashankar S A, *J Mater Chem B,* 2 (2014) 5585.
18 Majeed S, Bashir M & Shivashankar S A, *J Nanoparticle Res*, 17 (2015) 1.
19 Gai S, Li C, Yang P & Lin, J, *Chem Rev*,114 (2013) 2343.
20 Shen J, Sun L-D & Yan C-H, *Dalt Trans*, 42 (2008) 5687.
21 Chang C, Zhang Q & Mao D, *Nanotechnology*, 17 (2006) 1981.
22 Cao C, Yang H K, Chung J W, Moon B K, Choi B C, Jeong J H & Kim K H, *J Mater Chem*, 21 (2011) 10342.
23 Cheng S, Kam C & Buddhudu S, *Mater Res Bull*, 36 (2001) 1131.
24 Dong H, Du S, Zheng X, Lyu G, Sun L, Li L, Zhang P, Zhang C & Yan C, *Chem Rev*, 115 (2015) 10725.